$Cs_2InAgCl_6$: A new lead-free halide double perovskite with direct band gap

George Volonakis,[†] Amir Abbas Haghighirad,[‡] Rebecca L. Milot,[‡] Weng H. Sio,[†] Marina R. Filip,[†] Bernard Wenger,[‡] Michael B. Johnston,[‡] Laura M. Herz,[‡] Henry J. Snaith,[‡] and Feliciano Giustino*[,†]

†*Department of Materials, University of Oxford, Parks Road OX1 3PH, Oxford, UK*

‡*Department of Physics, Clarendon Laboratory, University of Oxford, Parks Road, Oxford OX1 3PU, United Kingdom*

E-mail: feliciano.giustino@materials.ox.ac.uk

Phone: (+44) 01865 272380

Abstract

$A_2BB'X_6$ halide double perovskites based on bismuth and silver have recently been proposed as potential environmentally-friendly alternatives to lead-based hybrid halide perovskites. In particular, Cs_2BiAgX_6 (X = Cl, Br) have been synthesized and found to exhibit band gaps in the visible range. However, the band gaps of these compounds are indirect, which is not ideal for applications in thin film photovoltaics. Here, we propose a new class of halide double perovskites, where the B^{3+} and B^{+} cations are In^{3+} and Ag^{+}, respectively. Our first-principles calculations indicate that the hypothetical compounds Cs_2InAgX_6 (X = Cl, Br, I) should all exhibit direct band gaps in the visible. Based on these predictions, we attempt to synthesize $Cs_2InAgCl_6$ and $Cs_2InAgBr_6$, and we succeed to form the hitherto unknown double perovskite $Cs_2InAgCl_6$. X-ray diffraction yields a double perovskite structure with space group $Fm\bar{3}m$. The compound is found to be photosensitive and turns reversibly from white to orange under ultraviolet illumination. We also perform an empirical analysis of the stability of Cs_2InAgX_6 and their mixed halides based on Goldschmidt's rules, and we find that it should also be possible to form $Cs_2InAg(Cl_{1-x}Br_x)_6$ for $x < 1$. The synthesis of mixed halides will open the way to the development of lead-free double perovskites with direct band gaps tunable across the visible range.

Table of Contents Image

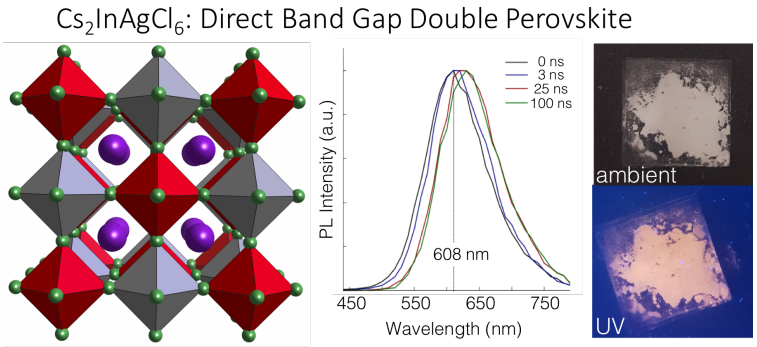

Keywords: In-based halide double perovskite, lead-free perovskite, direct bandgap, elpasolite.

During the last four years Pb-based halide perovskites have revolutionized the field of solution processable solar cells, achieving record power conversion efficiencies above 22%,[1] and surpassing polycrystalline and thin-film silicon photovoltaics (PV).[2–7] While the efficiency of these materials improves steadily, there are two remaining challenges that need to be addressed in order to use perovskite solar cells for electricity production, namely the compound stability and the presence of lead.[8] On the front of Pb replacement, several lead-free perovskites and perovskite-derivatives have been proposed during the past two years as potential substitutes for $MAPbI_3$ ($MA = CH_3NH_3$), including vacancy-ordered double perovskites, cation-ordered double perovskites (also known as elpasolites), and two-dimensional perovskites.[9–28] Among these compounds, Pb-free halide double perovskites based on Bi and Ag were recently proposed as stable and environmentally-friendly alternatives to $MAPbI_3$.[24–27] While these Bi/Ag double perovskites exhibit band gaps in the visible (from 1.9 to 2.2 eV, Ref. 27), the gaps are *indirect*, which is not ideal for thin film PV applications. In fact indirect band gaps imply weak oscillator strengths for optical absorption and for radiative recombination, therefore indirect semiconductors such as silicon need a much thicker absorber layer, which can be problematic if charge carriers mobilities are low. In order to circumvent this limitation, in this work we develop a new class of Pb-free halide double perovskites, which exhibit *direct* band gaps ~~in the visible~~. We first use available databases and first-principles calculations to identify double perovskites with direct band gaps, and then we synthesize and characterize the new In-based compound $Cs_2InAgCl_6$. X-ray diffraction (XRD) indicates a double perovskite structure with space group $Fm\bar{3}m$ at room temperature. Based on density-functional theory (DFT) we find a direct band gap of 2.6±0.5 eV.

The starting point of our investigation is the recent work on $Cs_2BiAgCl_6$ by some of us, Ref. 24. In that work we succeeded in synthesizing the new double perovskite $Cs_2BiAgCl_6$ by following the well-known reaction route for making $Cs_2BiNaCl_6$,[29] and by replacing the NaCl precursor by AgCl. The successful replacement of Na by Ag can be attributed to the

close match between the ionic radii of Na^+ (1.02 Å) and of Ag^+ (1.15 Å). Motivated by this observation, here we set to discover new halide double perovskites containing Ag. To this aim we search for known halide elpasolites containing Na^+ as the B^+ cation. We consider data from the Materials Project,[30] the International Crystal Structure Database (ICSD),[31] and literature reviews.[29,32–34] From Refs. 29,32–34 we find 42 elpasolites with composition $Cs_2B^{3+}NaX_6$, X = Cl, Br, I. In 30 of these compounds the B^{3+} cation is a lanthanide or actinide; in 7 compounds we find transition metals with small ionic radii (<0.9 Å), namely Sc, Ti, Y, and Fe; and 5 compounds contain Bi, Sb, Tl, or In. Lanthanides, actinides and transition metals pose a challenge to computational predictions based on DFT, therefore we leave them aside for future work. Bi and Sb double perovskites were extensively discussed in Ref. 24. The incorporation of Tl in halide double perovskites was proposed in Ref. 35, however this element is highly toxic and hence unsuitable for optoelectronic applications. Indium, on the other hand, is a common element in the optoelectronic industry, for example it is used to make transparent conductors in the form of tin doped indium oxide (ITO). Two In/Na-based halide double perovskites have been reported so far, $Cs_2InNaCl_6$[32,33] and $Cs_2InNaBr_6$.[33] Following this observation, we proceed to assess the structural, electronic, and optical properties of the hypothetical compounds Cs_2InAgX_6 with X = Cl, Br, I using DFT calculations.

As a structural template for our calculations we use the face-centered cubic $Fm\bar{3}m$ elpasolite unit cell, which contains one B^+X_6 and one $B^{3+}X_6$ octahedra.[24,26] The resulting atomistic model consists of InX_6 and AgX_6 octahedra which alternate along the [100], [010], and [001] directions, as shown in Figure 1a. This rock-salt ordering of the B-site cations is also found in many oxide double perovskites.[36] After optimizing the structure within the local density approximation (LDA) to DFT (see Methods), we obtain the lattice constants a = 10.20 Å, 10.74 Å, and 11.52 Å for X = Cl, Br, and I, respectively. The calculated lattice constants are slightly smaller than what we found for the corresponding Bi-based double perovskites (10.50-11.76 Å).[24] This can be attributed to the smaller size of In^{3+} as com-

pared to Bi^{3+}. Despite the presence of two different B-site cations, within DFT/LDA the BX_6 octahedra are of ~~very~~ similar size; for example in the case of $Cs_2InAgCl_6$ the In-Cl and Ag-Cl bond lengths are 2.50 Å and 2.59 Å, respectively. Employing higher level non-local functionals for the structural optimization yields a slightly larger lattice constant, 10.62 Å for $Cs_2InAgCl_6$, and bond lengths of 2.54 Å and 2.77 Å for In-Cl and Ag-Cl, respectively. All parameters related to structural optimization with different functionals are included in Table S1 of the Supporting Information.

A complete study of the stability of these hypothetical compounds would require the calculation of the phonon dispersion relations (dynamical stability) and of the quaternary convex hulls (thermodynamic stability).[37] Since these calculations are demanding, we perform a preliminary assessment of compound stability using Goldschmidt's empirical criteria.[38] According to these criteria, one can assign a perovskite with formula ABX_3 two parameters called the tolerance factor and the octahedral factor. The tolerance factor is defined as $t = (R_A + R_X)/\sqrt{2}(R_B + R_X)$, with R_A, R_B, and R_X the ionic radii of the elements in a ABX_3 perovskite; stable structures usually correspond to $0.75 < t < 1.0$.[39] The octahedral factor is defined as $\mu = R_B/R_X$, and stable structures tend to have $\mu > 0.41$.[40] In order to evaluate these parameters we employ the ionic radii from Ref. 41. Since we have double perovskites, and therefore different radii for the B^+ and B^{3+} sites, as a first attempt we consider for R_B the average between the radii of In^{3+} and Ag^+. For Cs_2InAgX_6 with X = Cl^-, Br^-, I^- we obtain $(\mu, t) = (0.54, 0.94)$, (0.50,0.93), and (0.44,0.91), respectively. All these parameters fall within the range of stability of standard halide perovskites,[39] therefore they are not very informative. A more stringent test can be obtained by considering the limiting cases where the structures were composed entirely of InX_6 octahedra or of AgX_6 octahedra. In this scenario we find that the tolerance factor is within the stability region for all compounds ($0.86 < t < 1.0$), but the octahedral factor μ is outside of this region for X = Br and I. The evolution of the octahedral factor as one moves from $Cs_2InAgCl_6$ to Cs_2InAgI_6 is shown in Figure 1b. It is apparent that the onset of the instability relates to

the InX_6 octahedra, and in particular to the fact that the ionic radius of In^{3+} is too small ($R_{In^{3+}} = 0.8$ Å) to coordinate 6 I^- anions ($R_{I^-} = 2.2$ Å). This analysis, albeit very crude, suggests that the only possible In/Ag halide double perovskites that may be amenable to synthesis are those with Cl, Cl/Br mixes, and possibly Br.

Guided by these results, we investigate the electronic structure of $Cs_2InAgCl_6$. In order to overcome the well-known limitations of DFT/LDA for the description of band gaps, we employ the HSE06 and the PBE0 hybrid functionals (see Methods). We perform calculations using both hybrid functionals since in our previous work on halide elpasolites[24,42] ~~we found that the PBE0 functional tends to overestimate the measured gaps, while HSE06 tends to slightly underestimate the gaps~~ (Table 1). ~~Therefore their combination should allow us to bracket the real band gap with a reasonable predictive power.~~ We also checked that, unlike in $MAPbI_3$,[43] spin-orbit effects are not important for In/Ag double perovskites, see Figure S1 of the Supporting Information. The band structure of $Cs_2InAgCl_6$ is shown in Figure 2a. The most striking finding is that the band gap is *direct*, with both valence and conduction band extrema at the center of the Brillouin zone (Γ point). The band gap is rather sensitive to the functional employed for the structural optimization (see Table S1), and range from 2.1 eV (LDA structure, HSE gap) to 3.1 eV (HSE structure and PBE0 gap). Given this uncertainty, we choose to report 2.6 ± 0.5 eV as the nominal band gap from the calculations.

In Table 1, we show the previously calculated[24,42] and measured[24–26,42] band gaps for the case of Cs_2BiAgX_6 (X = Cl, Br). The real band gaps are within the HSE06-PBE0 range, hence we expect a similar trend for $Cs_2InAgCl_6$. ~~Given that in the case of Cs_2BiAgX_6 (X = Cl, Br) the HSE06 band gaps proved to be closer to experiment (Table 1), we expect the real band gap of $Cs_2InAgCl_6$ to be in the vicinity of 2.1 eV.~~

In Figure 2b we show the square modulus of the electronic wavefunctions at the band edges. The bottom of the conduction band is mainly comprised of Cl-3p and In-5s/Ag-5s states, while the top of the valence band is derived from Cl-3p and In-4d/Ag-4d states. A detailed projected density of states and a qualitative molecular orbital diagram of $Cs_2InAgCl_6$

are shown in Figure S2 of the Supplementary Information. The valence band top of $Cs_2InAgCl_6$ has no occupied In-s orbitals. The absence of occupied s states is closely linked with the direct character of the band gap of this compound. In fact, in the related Bi/Ag elpasolite $Cs_2BiAgCl_6$,[24,42] the Bi s states at the top of the valence band interact with the directional Ag d states along the [100] direction; this interaction pushes the valence band top to the X point and leads to an indirect band gap in $Cs_2BiAgCl_6$. To confirm this point we artificially removed the Bi s states from the top of the valence band of $Cs_2BiAgCl_6$, using a fictitious Hubbard U correction of 10 eV. The resulting band structure, shown in Supplementary Figure S3, exhibits a direct gap at Γ, as in the case of the present compound $Cs_2InAgCl_6$.

The electron effective mass calculated for $Cs_2InAgCl_6$ is $m_e^* = 0.29\, m_e$ (m_e is the free electron mass); the hole effective mass is $m_h^* = 0.28\, m_e$. In the calculation of the hole effective mass we have not considered the non-dispersive band which can be seen in Figure 2a between Γ and X. This flat band originates from the hybridization of Cl-3$p_{x,y}$ states and 4$d_{x^2-y^2}$ states of In and Ag, which leads to a two-dimensional wavefunction confined within the equatorial (001) plane (wavefunction labelled as 'iii' in Figure 2b). This flat band will likely prevent carrier transport along the six equivalent X wavevectors, and possibly favor the formation of deep defects.

Since we expect $Cs_2InAgCl_6$ to be stable, and to exhibit a direct band gap as well as small and balanced effective masses, we proceed to attempt the synthesis of this compound. We prepare samples of $Cs_2BiAgCl_6$ by precipitation from an acidic solution of hydrochloric acid. A mixture of a 1 mmol $InCl_3$ (Sigma Aldrich, 99.99%) and AgCl (Sigma Aldrich, 99%) is first dissolved in 5 mL 10 M HCl. Then 2 mmol of CsCl (Sigma Aldrich, 99.9%) are added and the solution is heated to 115 °C. A white precipitate forms immediately after adding CsCl. We leave the hot solution for 30 min under gentle stirring, to ensure a complete reaction before filtering. We wash the resulting solid with ethanol and dry in a furnace overnight at 100 °C. The as-formed powder appears stable under ambient conditions.

In Figure 3a we show the measured X-ray diffraction (XRD) pattern of this powder. The refined lattice parameter is 10.47 Å, only 2.6% larger than in our DFT/LDA calculation. This is in line with the typical underestimation of lattice parameters by DFT/LDA in the range of 1-2%.[44] The refined structural parameters are provided in Table S2 of the Supporting Information. In Figure 3a we include the powder diffraction pattern calculated from our optimized DFT/LDA structure. We can see that all the peaks in the calculation and in the XRD measurement match very closely; there is a small offset between the two patterns, which is related to the difference in the lattice parameters. To confirm this point, we re-optimize the theoretical model using the experimental lattice constant; in this case we find no discernible difference between the two patterns, as shown in Figure S2a of the Supporting Information. This comparison indicates that the synthesized compound is a ~~ordered~~ double perovskite or elpasolite, within a $Fm\bar{3}m$ space group. While we can successfully synthesize $Cs_2InAgCl_6$, our preliminary attempts at making the related bromide compound, $Cs_2InAgBr_6$, have been unsuccessful thus far. In fact, by following a similar route as above, with CsBr instead of CsCl, we obtain a pale yellow powder that does not match the elpasolite $Fm\bar{3}m$ crystal structure.

In order to investigate whether the In and Ag cations are fully ordered, we have calculated the XRD pattern in three different scenarios: (1) using an ordered structure optimized within DFT/LDA, (2) using an ordered structure optimized with DFT/HSE, (3) using the measured lattice parameter and a perovskite structure with 0.5 In and 0.5 Ag occupations on the Wyckoff sites. The scenarios (1) and (2) are meant to describe a fully-ordered $Cs_2InAgCl_6$ crystal using DFT functionals which yield rather different In-Cl and Ag-Cl bond lengths (as shown in Table S1). These calculated XRD patterns are compared to experiment in Figure S5 of the Supplementary information. The main peaks associated with ordering effects are indicated by the green arrows in this figure. We find that the main peaks associated with ordering effects (indicated by the green arrows) are extremely weak even in the theoretical fully-ordered structures. Furthermore, we see that in the HSE structure these peaks are

slightly more visible than in the LDA structure. This effect is due to the more pronounced difference in bond lengths between In-Cl and Ag-Cl in the HSE structure (as seen in Table S1). In the fully-disordered model the intensity of the ordering peaks is vanishing. The difference between the XRD patterns calculated for the ordered structures (Figure S5b and S5c) and the disordered structure (Figure S5d) are much smaller than our experimental resolution (Figure S5a). Therefore, in the case of $Cs_2InAgCl_6$, XRD is not sufficient to probe the nature of cation order/disorder. Given this uncertainty on the structure, we explored the effects of disorder on the electronic structure. To this aim we considered a virtual crystal approximation with the In and Ag sites replaced by the pseudo-atom 0.5 In + 0.5 Ag. As shown in Figure S6, the DFT/HSE band structure of this disordered model is very close to that of the ordered model, with the same direct band gap at Γ. This demonstrates that our electronic structure analysis should be mostly insensitive to cation ordering.

In order to characterize the optical properties of $Cs_2InAgCl_6$, we measure the time-resolved photoluminescence (PL) spectra, and we estimate the absorbance by measuring the diffuse reflectance and applying the Kubelka-Munk theory (see Methods). In Figure 3b we see a well-defined PL peak centered around 608 nm (2.04 eV), with a FWHM of 120 nm (0.37 eV). This peak appears to redshift on a timescale of 100 ns, suggesting that subgap states are being filled on this timescale. The Kubelka-Munk function $F(R)$ is shown in Figure 3c. We can ~~clearly~~ recognize the onset of ~~band-to-band~~ absorption near 585 nm (2.12 eV). The Stokes shift (∼80 meV) between absorption and emission is comparable to that observed for lead-free $FASnI_3$ [FA = $CH(NH_2)_2$],[28] but significantly larger than that of high-quality $MAPbI_3$.[45] ~~Taken together, our PL and UV-Vis measurements indicate that $Cs_2InAgCl_6$ has a direct band gap of 2.1 eV.~~ A compound with the absorption onset and PL peak close to 2.1 eV, should be colored orange and not white as the $Cs_2InAgCl_6$ powder. However, we have observed that under photo-excitation the compound turns orange as shown in inset of Figure 3c. This coloration might relate to local photo-induced electronic or structural changes. For example, the precursor compound AgCl is a known photosensitive

material, where the oxidation state of Ag changes upon illumination. This photochromic behavior may be connected with the strong sensitivity of the electronic structure of $Cs_2InAgCl_6$ to small changes in the Ag-Cl and In-Cl bond lengths, as shown in Table S1 of the Supplementary Information. The process observed here is fully reversible and upon return to ambient light the sample becomes immediately white. The orange coloration is consistent with the optical absorption and emission spectra shown in Figure 3. Based on these observation we propose that the measured absorption and emission around 2.1 eV might relate to (possibly photo-induced) defect states. ~~In Figure 3b we also see optical activity below the absorption onset. This sub-gap absorption may be due to scatter from the powder sample or to color centers, although further work will be required to clarify this point.~~ In Figure 3d we see that the time-resolved PL intensity of $Cs_2InAgCl_6$ exhibits two timescales, a fast relaxation with a lifetime of 1 ns, followed by a very slow decay with a long lifetime of 6 μs. This observation is consistent with time-resolved PL measurements on the related Cs_2BiAgX_6 (X = Cl, Br) double perovskites, which also exhibit two decay components with very different lifetimes.[25] For completeness in Figure S2b of the Supporting Information we show that the PL lifetime is insensitive to the intensity of the pump laser. Taken together, the PL redshift with time, the moderate Stokes shift, and the fast initial PL decay component suggest that a tail of subgap defect states or energetic disorder is present. Elimination of such states may lead to longer overall PL lifetimes.

We employ DFT to compare the *ideal* optical absorption spectrum of $Cs_2InAgCl_6$ and $Cs_2InAgBr_6$ with the spectra calculated for the standard semiconductors Si and GaAs,[46] and for $MAPbI_3$ (unpublished results). In Figure 4a we see that, while $Cs_2InAgCl_6$ is a direct-gap semiconductor, its absorption coefficient is considerably smaller than those of Si, GaAs, and $MAPbI_3$ throughout the visible spectrum. On the other hand, if we could synthesize the bromine compound, $Cs_2InAgBr_6$, we should obtain an absorption coefficient which is comparable or even higher than silicon.

In view of developing more efficient absorbers based on the In/Ag combination, we

theoretically investigate the optical properties of mixed halide compounds. To this aim we consider the hypothetical solid solutions $Cs_2InAg(Cl_{1-x}Br_x)_6$, $Cs_2InAg(Br_{1-x}I_x)_6$ and $Cs_2InAg(Cl_{1-x}I_x)_6$ with $x = 0.25$, 0.50, and 0.75. To model mixed-halide double perovskites without inducing artificial ordering effects, we employ the virtual-crystal approximation (see Methods). Figure 4b shows a ternary map of the band gap calculated for these mixes, as obtained by interpolating linearly from the above combinations. We report band gaps calculated using DFT/HSE06 and DFT/PBE0 ~~since this yields good agreement with our experiments~~ for $Cs_2InAgCl_6$. The band gaps of the mixed halide double perovskites are highly tunable within all the visible spectrum. ~~Assuming From this map we see that it should be possible to obtain a gap below 2 eV by incorporating 15% of Br (molar ratio) or 5% of I in $Cs_2InAgCl_6$. Similarly, by making a compound with 33% of Cl, Br, and I, it should be possible to obtain a band gap as low as 1 eV.~~ These results indicate that the the In/Ag halide double perovskites may be promising for applications in tandem solar cell architectures.[7]

In summary, by combining first-principles calculations and experiments we discovered a novel direct band gap halide double perovskite, $Cs_2InAgCl_6$. This new compound crystallizes in a double perovskite structure with space group $Fm\bar{3}m$, and has a direct band gap at Γ ~~of 2.1 eV~~ of 2.6±0.5 eV, as well as small and balanced electron and hole effective masses, required for high charge-carrier mobilities. In addition, this new compound shows an interesting photochromic behavior whereby the color changes reversibly to orange under UV illumination. Our analysis indicates that by developing mixed halides Cs_2InAgX_6 with X = Cl, Br, and I, it should be possible to obtain good optical absorbers and electron/hole conductors with tunable and direct band gaps. The existence of the related compound $Cs_2InNaBr_6$ (with Na in place of Ag) strongly suggests that it should be viable to synthesize also $Cs_2InAgBr_6$. Overall, we expect that the exploration of mixed-halide double perovskites starting from $Cs_2InAgCl_6$ will offer new opportunities for developing environmentally friendly perovskite photovoltaics and optoelectronics.

Computational Methods: Structural optimization was carried out within DFT using the

Quantum ESPRESSO suite.[47] Ultrasoft pseudopotentials[48,49] were used to describe the electron-ion interaction, and exchange-correlation effects were taken into account within the LDA.[50,51] The planewaves kinetic energy cutoffs were set to 35 Ry and 280 Ry for the electronic wavefunctions and the charge density, respectively. The Brillouin zone was sampled using a 15×15×15 unshifted grid. The thresholds for the convergence of forces and total energy were set to 10^{-3} Ry and 10^{-4} Ry, respectively. In order to overcome the DFT band gap problem we employed hybrid functional calculations as implemented in the VASP code.[52] We used the PBE0 functional[53] and the HSE06 functional.[54] In the latter case we set the screening parameter to 0.2 Å^{-1} and we used a mixing of 25% of Fock exchange with 75% of PBE exchange. In the hybrid calculations we used the projector augmented wave method,[55] with a 400 eV kinetic energy cutoff. In the hybrid calculations the Brillouin zone was sampled using a 6×6×6 unshifted grid for Cl or Br. For the I-based compound, Cs_2InAgI_6, DFT/LDA yields a spurious band crossing and the resulting band structure is metallic. In this case, in order to perform hybrid calculations we sampled the Brillouin zone using a 2×2×2 shifted grid. We verified the correctness of the results by repeating the same procedure for $Cs_2InAgCl_6$. For the calculations of the optical absorption coefficients we used the YAMBO code[56] within the random-phase approximation. In this case we used norm-conserving pseudopotentials[57] (with kinetic energy cutoff of 120 Ry), the PBE[58] generalized gradient approximation, and a dense Brillouin zone grid with 40×40×40 points. In order to correct for the band gap underestimation in DFT/PBE we used scissor corrections as obtained from our HSE06 calculations. The optical f-sum rule was maintained by scaling the oscillator strengths, following Ref. 59. The calculations based on the virtual-crystal approximation were performed by using the procedure of Ref. 60. All figures involving atomic structures were rendered using VESTA.[61]

Experimental Methods: Powder XRD was performed using a Panalytical X'pert diffractometer (Cu-Kα_1 radiation; $\lambda = 154.05$ pm) at room temperature. Structural parameters were obtained by Rietveld refinement using the General Structural Analysis Software.[62,63] A Varian

Cary 300 UV-Vis spectrophotometer with an integrating sphere was used to acquire diffuse reflectance. To estimate the visible light absorption spectrum, we apply the Kubelka-Munk theory to convert the diffuse reflectance in the $F(R)$ function, $F(R) = (1-R)^2/2R = K/S$, where R is the absolute reflectance of the sample, K is the molar absorption coefficient, and S is the scattering coefficient.Time-resolved PL spectra were recorded following laser excitation at 405 nm, at a repetition rate of 10 MHz (Picoquant, LDH-D-C-405M). The PL signal was collected and directed toward a grating monochrometer (Princeton Instruments, SP-2558), and detected with a photon-counting detector (PDM series from MPD).

Acknowledgement

G.V., W.H.S., M.R.F., and F.G. would like to thank Marios Zacharias for sharing the calculated absorption coefficients of Si, GaAs and $MAPbI_3$. The research leading to these results has received funding from the Graphene Flagship (Horizon 2020 grant no. 696656 - GrapheneCore1), the Leverhulme Trust (Grant RL-2012-001), the UK Engineering and Physical Sciences Research Council (Grant No. EP/J009857/1, EP/M020517/1 and EP/L024667/1). The authors acknowledge the use of the University of Oxford Advanced Research Computing (ARC) facility (http://dx.doi.org/10.5281/zenodo.22558) and the ARCHER UK National Supercomputing Service under the 'AMSEC' Leadership project and PRACE for awarding us access to the Dutch national supercomputer 'Cartesius'.

References

(1) Best Research-Cell Efficiencies. `http://www.nrel.gov/`.

(2) Xing, G.; Mathews, N.; Sun, S.; Lim, S. S.; Lam, Y. M.; Grätzel, M.; Mhaisalkar, S.; C., S. T. *Science* **2013**, *342*, 344.

(3) Stranks, S. D.; Grancini, G. E.; Menelaou, G.; Alcocer, C.; Leijtens, M. J. P.; M., H. L.; Petrozza, A.; Snaith, H. J. *Science* **2013**, *342*, 341.

(4) Sum, T. C.; Mathews, N. *Energ. Environ. Sci.* **2014**, *7*, 2518.

(5) Wehrenfennig, C.; Eperon, G. E.; Johnston, M. B.; Snaith, H. J.; Herz, L. M. *Adv. Mater.* **2014**, *26*, 1584.

(6) Seo, J.; Noh, J. H.; Seok, S. I. *Accounts of Chemical Research* **2016**, *49*, 562–572.

(7) Eperon, G. E. et al. *Science* **2016**,

(8) Green, M.; Ho-Baillie, A.; Snaith, H. J. *Nature Photonics* **2014**, *8*, 506.

(9) Stoumpos, C. C.; Malliakas, C. D.; Kanatzidis, M. G. *Inorg. Chem.* **2013**, *52*, 9019.

(10) Noel, N.; Stranks, S. D.; Abate, A.; Wehrenfennig, C.; Guarnera, S.; Haghighirad, A.-A.; Sadhanala, A.; Eperon, G. E.; Pathak, S. K.; Johnston, M. B.; Petrozza, A.; Herz, L. M.; Snaith, H. J. *Energ. Environ. Sci* **2014**, *7*, 3061.

(11) Hao, F.; Stoumpos, C. C.; Cao, D. H.; Chang, R. P. H.; Kanatzidis, M. G. *Nature Photonics* **2014**, *8*, 489.

(12) Lee, B.; Stoumpos, C. C.; Zhou, N.; Hao, F.; Malliakas, C.; Yeh, C.-Y.; Marks, T. J.; Kanatzidis, M. G.; Chang, R. P. H. *J. Am. Chem. Soc.* **2014**, *136*, 15379–15385.

(13) Maughan, A. E.; Ganose, A. M.; Bordelon, M. M.; Miller, E. M.; Scanlon, D. O.; Neilson, J. R. *J. Am. Chem. Soc.* **2016**, *138*, 8453–8464.

(14) Kaltzoglou, A.; Antoniadou, M.; Perganti, D.; Siranidi, E.; Raptis, V.; Trohidou, K.; Psycharis, V.; Kontos, A. G.; Falaras, P. *Electrochim. Acta* **2015**, *184*, 466–474.

(15) Kaltzoglou, A.; Antoniadou, M.; Kontos, A. G.; Stoumpos, C. C.; Perganti, D.; Siranidi, E.; Raptis, V.; Trohidou, K.; Psycharis, V.; Kanatzidis, M. G.; Falaras, P. *J. Phys. Chem. C* **2016**, *120*, 11777–11785.

(16) Saparov, B.; Hong, F.; Sun, J.-P.; Duan, H.-S.; Meng, W.; Cameron, S.; Hill, I. G.; Yan, Y.; Mitzi, D. B. *Chem. Mater.* **2015**, *27*, 5622–5632.

(17) Park, B.-W.; Philippe, B.; Zhang, X.; Rensmo, H.; Boschloo, G.; Johansson, E. M. J. *Adv. Mater.* **2015**, *27*, 6806–6813.

(18) Hebig, J.-C.; Kühn, I.; Flohre, J.; Kirchartz, T. *ACS Energy Lett.* **2016**, *1*, 309–314.

(19) Singh, T.; Kulkarni, A.; Ikegami, M.; Miyasaka, T. *ACS Appl. Mater. Interfaces* **2016**, *8*, 14542–14547.

(20) Harikesh, P. C.; Mulmudi, H. K.; Ghosh, B.; Goh, T. W.; Teng, Y. T.; Thirumal, K.; Lockrey, M.; Weber, K.; Koh, T. M.; Li, S.; Mhaisalkar, S.; Mathews, N. *Chem. Mater.* **2016**, *28*, 7496–7504.

(21) Kim, Y.; Yang, Z.; Jain, A.; Voznyy, O.; Kim, G.-H.; Liu, M.; Quan, L. N.; GarcadeArquer, F. P.; Comin, R.; Fan, J. Z.; Sargent, E. H. *Angew. Chem.* **2016**, *128*, 9738–9742.

(22) Xiao, Z.; Meng, W.; Mitzi, D. B.; Yan, Y. *J. Phys. Chem. Lett.* **2016**, *7*, 3903–3907.

(23) Fabian, D. M.; Ardo, S. *J. Mater. Chem. A* **2016**, *4*, 6837–6841.

(24) Volonakis, G.; Filip, M. R.; Haghighirad, A. A.; Sakai, N.; Wenger, B.; Snaith, H. J.; Giustino, F. *J. Phys. Chem. Lett.* **2016**, *7*, 1254–1259.

(25) Slavney, A. H.; Hu, T.; Lindenberg, A. M.; Karunadasa, H. I. *J. Am. Chem. Soc.* **2016**, *138*, 2138–2141.

(26) McClure, E. T.; Ball, M. R.; Windl, W.; Woodward, P. M. *Chem. Mater.* **2016**, *28*, 1348–1354.

(27) Filip, M. R.; Giustino, F. *J. Phys. Chem. C* **2016**, *120*, 166–173.

(28) Milot, R. L.; Eperon, G. E.; Green, T.; Snaith, H. J.; Johnston, M. B.; Herz, L. M. *J. Phys. Chem. Lett.* **2016**, *7*, 4178–4184.

(29) Morss, L. R.; Robinson, W. R. *Acta Cryst. B* **1972**, *28*, 653–654.

(30) Jain, A.; Ong, S. P.; Hautier, G.; Chen, W.; Richards, W. D.; Dacek, S.; Cholia, S.; Gunter, D.; Skinner, D.; Ceder, G.; Persson, K. A. *APL Mater.* **2013**, *1*, 011002.

(31) Inorganic Crystal Structure Database, FIZ Karlsruhe: Germany. `http://www2.fiz-karlsruhe.de`.

(32) Morss, L. R.; Siegal, M.; Stenger, L.; Edelstein, N. *Inorg. Chem.* **1970**, *9*, 1771–1775.

(33) Meyer, G.; Gaebell, H. *Z. Naturforsch. B* **1978**, *33*, 1476–1478.

(34) Meyer, G. *Z. Naturforsch. B* **1980**, *35*, 268–276.

(35) Giorgi, G.; Yamashita, K. *Chem. Lett.* **2015**, *44*, 826.

(36) Vasala, S.; Karppinen, M. *Prog. Solid State Chem.* **2015**, *4*, 1–36.

(37) Hautier, G.; Ong, S. P.; Jain, A.; Moore, C. J.; Ceder, G. *Phys. Rev. B* **2012**, *85*, 155208.

(38) Goldschmidt, V. M. *Berichte der deutschen chemischen Gesellschaft (A and B Series)* **1927**, *60*, 1263–1296.

(39) Li, C.; Lu, X.; Ding, W.; Feng, L.; Gao, Y.; Guo, Z. *Acta Cryst. B* **2008**, *64*, 702–707.

(40) Rohrer, G. *Structure and Bonding in Crystalline Materials*; Cambridge University Press: Cambridge, 2001.

(41) Shannon, R. D. *Acta. Cryst. A* **1976**, *32*, 751–767.

(42) Filip, M. R.; Hillman, S.; Haghighirad, A. A.; Snaith, H. J.; Giustino, F. *J. Phys. Chem. Lett.* **2016**, *7*, 2579–2585.

(43) Even, J.; Pedesseau, L.; Jancu, J.-M.; Katan, C. *J. Phys. Chem. Lett.* **2013**, *4*, 2999.

(44) Giustino, F. *Materials Modelling Using Density Functional Theory: Properties and Predictions*; Oxford University Press: Oxford, 2014.

(45) Milot, R. L.; Eperon, G. E.; Snaith, H. J.; Johnston, M. B.; Herz, L. M. *Advanced Functional Materials* **2015**, *25*, 6218–6227.

(46) Zacharias, M.; Giustino, F. *Phys. Rev. B* **2016**, *94*, 075125.

(47) Giannozzi, P. et al. *J. Phys.: Condens. Matter.* **2009**, *21*, 395502.

(48) Rappe, A. M.; Rabe, K. M.; Kaxiras, E.; Joannopoulos, J. D. *Phys. Rev. B* **1990**, *41*, 1227.

(49) Vanderbilt, D. *Phys. Rev. B* **1990**, *41*, 7892.

(50) Ceperley, D. M.; Alder, B. J. *Phys. Rev. Lett.* **1980**, *45*, 566.

(51) Perdew, J. P.; Zunger, A. *Phys. Rev. B* **1981**, *23*, 5048.

(52) Kresse, G.; Furthmuller, J. *Phys. Rev. B* **1996**, *54*, 11169–11186.

(53) Paier, J.; Hirschl, R.; Marsman, M.; Kresse, G. *J. Chem. Phys.* **2005**, *122*, 234102.

(54) Krukau, A. V.; Vydrov, O. A.; Izmaylov, A. F.; Scuseria, G. E. *J. Chem. Phys.* **2006**, *125*, 224106.

(55) Blöchl, P. E. *Phys. Rev. B* **1994**, *50*, 17953–17979.

(56) Marini, A.; Hogan, C.; Grüning, M.; Varsano, D. *Comp. Phys. Commun.* **2009**, *180*, 1392.

(57) Troullier, N.; Martins, J. L. *Phys. Rev. B* **1991**, *43*, 1993.

(58) Perdew, J. P.; Burke, K.; Ernzerhof, M. *Phys. Rev. Lett.* **1996**, *77*, 3865.

(59) Zacharias, M.; Patrick, C. E.; Giustino, F. *Phys. Rev. Lett.* **2015**, *115*, 177401.

(60) Bellaiche, L.; Vanderbilt, D. *Phys. Rev. B* **2000**, *61*, 7877.

(61) Momma, K.; Izumi, F. *J. Appl. Cryst.* **2008**, *41*, 653.

(62) Larson, A. C.; Von Drele, R. B. *Los Alamos National Laboratory Report LAUR* **2000**, 86–748.

(63) Toby, B. H. *J. Appl. Cryst.* **2001**, *34*, 210–234.

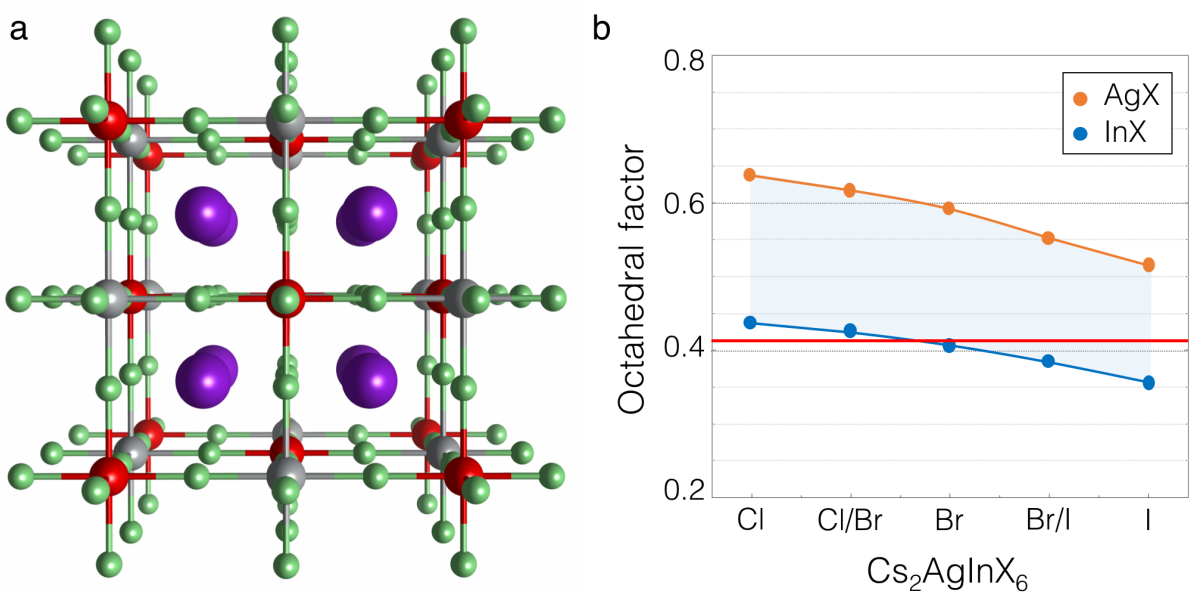

Figure 1: **Atomistic model and octahedral factors of the In-based halide double perovskites Cs_2InAgX_6 (X = Cl, Br, I)**: (a) Ball-and-stick model of $Cs_2InAgCl_6$, with In atoms in red and Ag atoms in gray. The green spheres indicate Cl, and the purple spheres in the center of each cavity are Cs atoms. The primitive unit cell contains one $InCl_6$ and one $AgCl_6$ octahedra in a face-centered cubic structure, with space group $Fm\bar{3}m$; here we show the conventional cubic cell. (b) Octahedral factor $\mu = R_B/R_X$ corresponding to AgX_6 octahedra (orange dots), and to InX_6 octahedra (blue dots), for solid solutions of Cl, Br, and I. The perovskite structure is expected to be unstable for values of the octahedral factor below $\mu = \sqrt{2} - 1 = 0.41$, as indicated by the red horizontal line.[39]

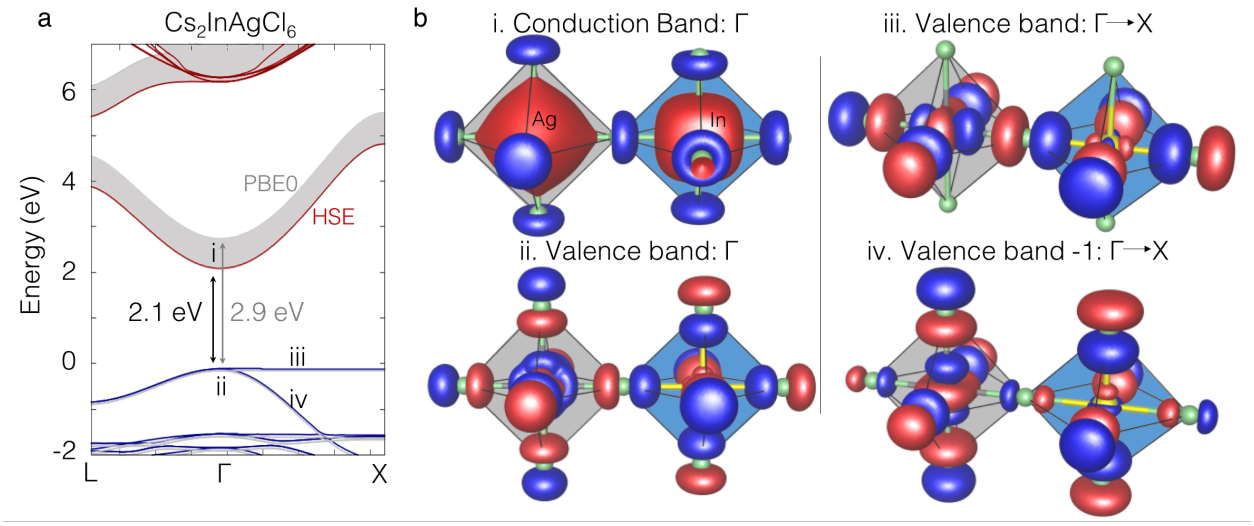

Figure 2: **Electron band structure and square modulus of the wavefunctions for $Cs_2InAgCl_6$**: (a) Band structures and band gaps of $Cs_2InAgCl_6$, as calculated by using the HSE06 hybrid functional (blue and red lines) or the PBE0 functional (shaded area). The zero of the energy scale is set to the top of the valence band. (b) Isosurface plots of the square modulus of the Kohn-Sham wavefunctions corresponding to (i) the bottom of the conduction band at Γ; (ii) the sum of the two degenerate states at the valence band top at Γ; (iii) the highest occupied state along the ΓX line, for a wavevector $\mathbf{k} \to \Gamma$ (0.2 ΓX); the second-highest occupied state along ΓX, for $\mathbf{k} \to \Gamma$ (0.2 ΓX).

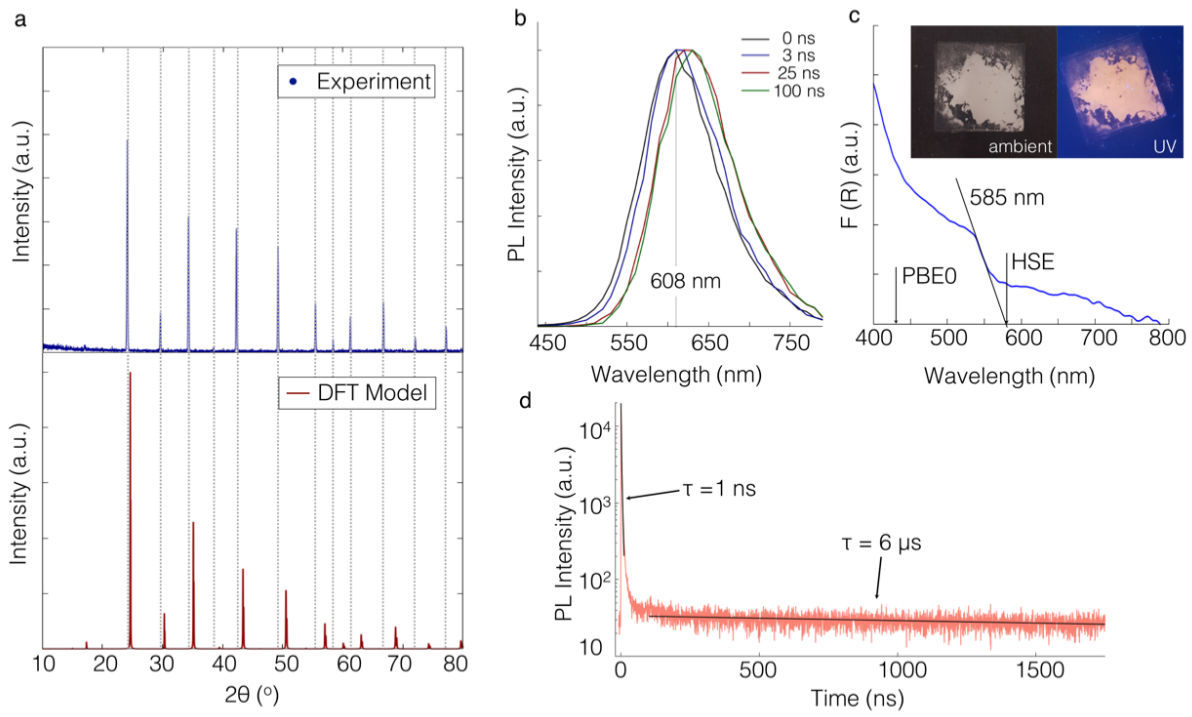

Figure 3: **Structural and optical characterization of $Cs_2InAgCl_6$**: (a) Measured powder XRD pattern for the as-synthesized $Cs_2InAgCl_6$ (top), and the XRD pattern calculated from the atomistic model optimized using DFT/LDA (bottom). (b) Normalized PL spectrum recorded as a function of time following excitation at 405 nm. The vertical line indicates the centre wavelength of the PL at zero time, defined by the arrival time of the excitation pulse on the sample. (c) Measured UV-Vis absorbance. The arrows show the calculated band gaps within the HSE and PBE0 hybrid functionals. The straight line is a guide to the eye. The inset shows $Cs_2InAgCl_6$ under ambient light and under UV illumination. (d) Time-resolved PL intensity recorded for a powder sample of $Cs_2InAgCl_6$. The fast and slow components of the PL decay are indicated on the plot. The fast (slow) component was fit with a stretched exponential (monoexponential) function, and τ represents the average lifetime.

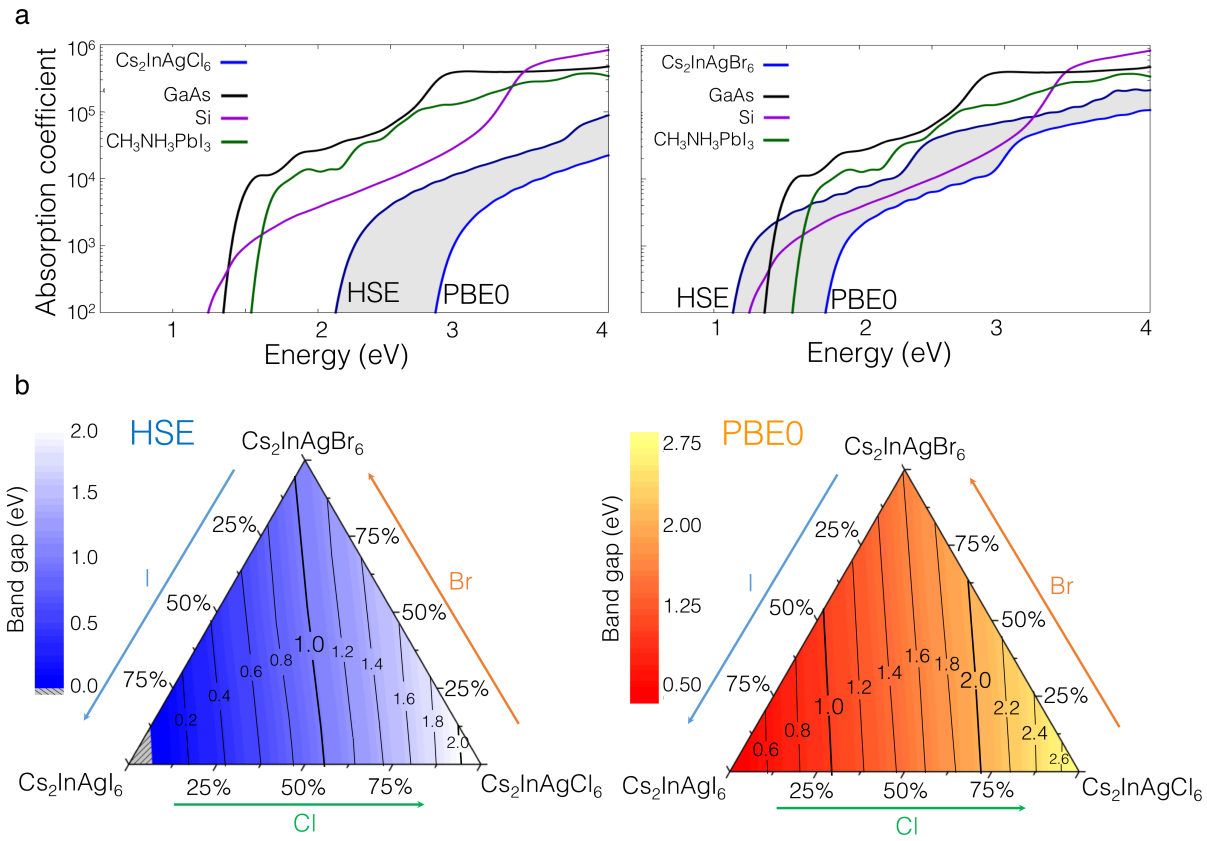

Figure 4: **Theoretical optical absorption coefficient and band gap of mixed halides**: (a) Calculated absorption coefficient of the compound synthesized in this work, $Cs_2InAgCl_6$ (left, blue lines), and of the hypothetical compound $Cs_2InAgBr_6$ (right, blue lines). For comparison we show the theoretical absorption coefficients of silicon (purple), gallium arsenide (black), as calculated in Ref. 46, and $MAPbI_3$ (green) (unpublished results). (b) Calculated band gaps of hypothetical mixed-halide double perovskites $Cs_2InAg(Cl_{1-x-y}Br_xI_y)_6$ within the HSE (left) and PBE0 (right) hybrid functional. The corners of the triangle correspond to Cs_2InAgX_6 with X = Cl, Br, I.

Table 1: **Comparison between calculated and measured band gaps of halide double perovskites**: The first column reports our present results for $Cs_2InAgCl_6$ (HSE06 and PBE0 calculations, for the structure optimized using LDA; values obtained for structures optimized using PBE, HSE, and PBE0 are given in Table S1), the second and third columns report PBE0 calculations and measurements on $Cs_2BiAgCl_6$ and $Cs_2BiAgBr_6$ from Refs. 24, 25, 26 and 42. The HSE06 calculations are from this work.

	$Cs_2InAgCl_6$	$Cs_2BiAgCl_6$	$Cs_2BiAgBr_6$
HSE06	2.1	2.1	1.7
PBE0	2.9	2.7	2.3
Exp.	~~2.1~~	2.2-2.8	1.9-2.2